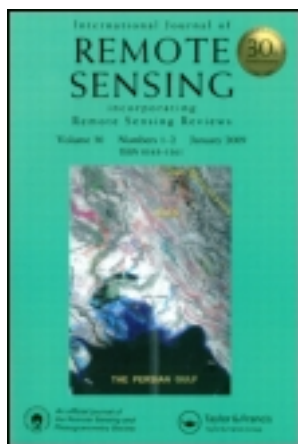


This article was downloaded by: [Lib4RI]

On: 24 October 2011, At: 23:19

Publisher: Taylor & Francis

Informa Ltd Registered in England and Wales Registered Number: 1072954 Registered office: Mortimer House, 37-41 Mortimer Street, London W1T 3JH, UK



## International Journal of Remote Sensing

Publication details, including instructions for authors and subscription information:

<http://www.tandfonline.com/loi/tres20>

### Deriving fine-scale socioeconomic information of urban areas using very high-resolution satellite imagery

Francisco J. Tapiador<sup>a</sup>, Sylvania Avelar<sup>b</sup>, Carlos Tavares-Corrêa<sup>c</sup> & Rainer Zah<sup>d</sup>

<sup>a</sup> Institute of Environmental Sciences (ICAM), University of Castilla-La Mancha (UCLM), Avenida Carlos III s/n, 45071, Toledo, Spain

<sup>b</sup> Media Technology Laboratory, Swiss Federal Laboratories for Materials Testing and Research (Empa), Überlandstrasse 129, CH-8600, Dübendorf, Switzerland

<sup>c</sup> Applied Geography Research Center, Pontifical Catholic University of Peru (PUCP), Av. Universitaria 1801, San Miguel, Lima, 32, Peru

<sup>d</sup> Technology and Society Laboratory, Swiss Federal Laboratories for Materials Testing and Research (Empa), Überlandstrasse 129, CH-8600, Dübendorf, Switzerland

Available online: 02 Aug 2011

To cite this article: Francisco J. Tapiador, Sylvania Avelar, Carlos Tavares-Corrêa & Rainer Zah (2011): Deriving fine-scale socioeconomic information of urban areas using very high-resolution satellite imagery, International Journal of Remote Sensing, 32:21, 6437-6456

To link to this article: <http://dx.doi.org/10.1080/01431161.2010.512928>

PLEASE SCROLL DOWN FOR ARTICLE

Full terms and conditions of use: <http://www.tandfonline.com/page/terms-and-conditions>

This article may be used for research, teaching, and private study purposes. Any substantial or systematic reproduction, redistribution, reselling, loan, sub-licensing, systematic supply, or distribution in any form to anyone is expressly forbidden.

The publisher does not give any warranty express or implied or make any representation that the contents will be complete or accurate or up to date. The accuracy of any instructions, formulae, and drug doses should be independently verified with primary sources. The publisher shall not be liable for any loss, actions, claims, proceedings, demand, or costs or damages whatsoever or howsoever caused arising directly or indirectly in connection with or arising out of the use of this material.

## Deriving fine-scale socioeconomic information of urban areas using very high-resolution satellite imagery

FRANCISCO J. TAPIADOR\*†, SILVANIA AVELAR‡, CARLOS TAVARES-CORRÊA§ and RAINER ZAH¶

†Institute of Environmental Sciences (ICAM), University of Castilla-La Mancha (UCLM), Avenida Carlos III s/n, 45071, Toledo, Spain

‡Media Technology Laboratory, Swiss Federal Laboratories for Materials Testing and Research (Empa), Überlandstrasse 129, CH-8600 Dübendorf, Switzerland

§Applied Geography Research Center, Pontifical Catholic University of Peru (PUCP), Av. Universitaria 1801, San Miguel, Lima 32, Peru

¶Technology and Society Laboratory, Swiss Federal Laboratories for Materials Testing and Research (Empa), Überlandstrasse 129, CH-8600 Dübendorf, Switzerland

(Received 17 July 2008; in final form 23 July 2010)

This article presents a new approach to derive fine-scale socioeconomic information of urban areas using very high resolution satellite data. The rationale behind the method is to use high resolution satellite data, capable of resolving urban morphology details, to derive a classification of the image. Thus, it is assumed that there is a relationship between the socioeconomic profile and the urban morphology of an area in terms of availability of green areas, sport facilities, private swimming pools or pavement conditions. The method is tested using a case study of Lima, Peru. Using a sample of ground data, a neural network classifier was applied to a pre-classified image in which entropy had been used to mask extensive, non-built up areas that would otherwise have inserted spurious information into the classifier. The result shows a high correlation ( $0.70 R^2$ ) when compared with validation data. The good performances also show that a physiographic satellite view of the city reflects the socioeconomic layout of their inhabitants, thus making remote sensing a complementary tool for social research and urban planning. While the parameterization of the problem may differ from one area to another, it is shown that an *a priori* choice of a few parameters may help to automatically characterize large areas in social terms, thus allowing social inequality and its evolution to be mapped in those areas with limited availability of data. In order to make the method widely applicable, the possibilities and limitations of applying the procedure to other large cities are discussed.

### 1. Introduction

Remote sensing can be used to provide up-to-date spatial information of a wide variety of urban phenomena at multiple resolutions (Jensen and Cowen 1999, Herold *et al.* 2007, Wang and Quattrochi 2007). To that end, both active and passive sensors have been used: satellite data can be used to detect settlements using synthetic

---

\*Corresponding author. Email: francisco.tapiador@uclm.es

aperture radar (SAR, Henderson and Xia 1997) while high-resolution, passive sensors such as Landsat Thematic Mapper (TM)/Enhanced Thematic Mapper (ETM) or Satellite pour l'Observation de la Terre (SPOT) have also been widely used to map socioeconomic parameters. Strategies for characterizing urban/non urban areas and urban characteristics include the use of nocturnal city lights (Doll *et al.* 2000), vegetation indexes (Lo 2002, Jensen *et al.* 2004), and Net Primary Production (NPP, Brown 2006). The advantages of satellite data for urban studies are obvious: images offer wide coverage, providing objective, cost-effective physical measurements over an extended period of time.

Nonetheless, the accurate classification of urban land cover and land use categories from very high resolution (higher than 1 m) imagery data remains a challenge (Fox *et al.* 2003). One of the reasons is the difficulty in defining suitable training sets for a supervised classification, since various land cover types co-exist and alternate frequently, for example, roads, sidewalks, houses, trees, bare soil and swimming pools, and their elements themselves present heterogeneity, such as a road with cars, resulting in distinct spectral variation within areas of homogeneous land cover classes (Taubenbock *et al.* 2006). In spite of recent advances (Wu 2004, Fauvel *et al.* 2006) additional difficulties arise when considering the dissimilarity of functions for inferring urban land use, such as residential or industrial areas, parks or agricultural fields. The distinction between land cover and land use has often been overlooked in urban studies (Mesev 2003): the correspondence between land use and land cover is not a one-to-one relationship as for example the land use classes of gardens, houses, and canals may refer to land cover classes of vegetation, buildings, and water, respectively. This makes assigning classified images to land uses a non trivial task (Foody 2002, Huang *et al.* 2002).

The task of deriving socioeconomic information from satellite imagery is also paved with obvious difficulties, as any relationship between radiometric values and social characteristics has to rely on an indirect procedure. Nevertheless, successful attempts to extract socioeconomic information from satellites or to link imagery with census data have been described. Thus, Li and Weng (2007) measured quality of life using Landsat ETM and the US census 2000 as did Lo and Faber (1997), the former using geophysical parameters such as the Normalized Difference Vegetation Index (NDVI) and surface temperature. Another approach was followed by Jensen *et al.* (2004) by using urban leaf area and population density to infer quality of life using a simple least-square regression, which illustrates the existence of an indirect relationship between social well-being and satellite data. The relevance of satellite data for landscape and urban planning studies is clear: the integration of satellite imagery with population census data has been used for studying the present human environment (Martinuzzi *et al.* 2007), and the usefulness of satellite technology for modelling the future trends in city growth has been explored by Weber (2003). The potential links between socioeconomic classes and land cover have been analysed by Avelar *et al.* (2009).

This article presents an attempt to derive socioeconomic information from satellite data using a new methodology. The aim is to derive a fine-scale socioeconomic classification of urban areas with a minimum set of *a priori* information to make the procedure as general as possible. This can help to apply the method to different areas, especially in large cities of developing countries, where contrasting socioeconomic classes co-exist and can be correlated to different urban conditions and spatial patterns.

## 2. Data

A QuickBird satellite image was used as the empirical basis for a case study in Lima, Peru. The image was taken on 28 February 2005. The radiometric resolution of QuickBird data is 11 bits thus allowing  $2^{11}$  digital counts for each pixel. The spatial resolution of this satellite is 0.6 m for a panchromatic image and 2.4 m for multispectral bands. The high spatial resolution of the panchromatic image makes it possible to distinguish small elements such as small swimming pools or tennis courts that multispectral bands cannot fully resolve. QuickBird multispectral images have three visible bands ( $b_1$ , blue: 0.45–0.52  $\mu\text{m}$ ,  $b_2$ , green: 0.52–0.60  $\mu\text{m}$ ,  $b_3$ , red: 0.63–0.69  $\mu\text{m}$ ) and one near-infrared band ( $b_4$  at 0.76–0.90  $\mu\text{m}$ ). Therefore, a  $b_3/b_2/b_1$  RGB (red/green/blue) combination gives a real colour view of the ground. Pan-sharpened products are available only from imagery acquired after 9 April 2002.

Figure 1 depicts an overview of the study area with some zooms identifying urban areas with different socioeconomic characteristics. The area corresponds to the Santiago de Surco sector of Lima city in Peru. Ground data were uniformly sampled around the city using Global Positioning System (GPS) to geolocate the estimates. The information collected was representative for an approximate radius of 50 m around the assigned coordinate while the GPS precision was about 15 m. In the end, 500 sample points were taken, 100 for each socioeconomic class. Figure 2 shows representative ground pictures of some of those classes.

While general social classifications in urban systems exist (e.g. Seto and Kaufman 2003, Pozzi and Small 2005), the official classes used by the city planners were used here. Thus, a nominal scale from A to E is used to categorize the inhabitants, with the A social class representing the most accommodated people and E for the poorest social class. The five A, B, C, D, E socioeconomic classes are assigned based upon the observations of existing buildings, including dwelling size, number of floors, build density, presence or absence of green areas, street pavement and land use. These characteristics are the physiographic characteristics corresponding to the standard statistical census categories on social classes of Lima, which are described in table 1.

The ground data were collected on 21–27 August 2005, in a  $9 \times 10$  km area in the south of Lima. The study area was divided into six equal sectors that were surveyed by two female and two male geography students working in pairs. Sample points were selected in homogeneous social areas, independent of the land use, and in critical areas such as slopes, unpaved streets, and non-built up areas. However, homogeneity was sometimes difficult to obtain because of the variety of constructions, building materials, surfaces, etc. The sample points were reached by car or walking, depending on the accessibility and safety to move freely around specific areas of the district.

## 3. Methods

Figure 3 schematically describes the methodology. The procedure is as follows. (1) First, improve the spatial resolution of the multispectral data by inserting the physiographic information of the panchromatic band through a data-fusion method (section 3.1). (2) Then, classify the fused image using a Mahalanobis distance algorithm. Within this step, a consistency matrix is used to check that each socioeconomic class has a unique signature in terms of satellite observables (section 3.2). (3) The next step is to calculate the entropy of the image (section 3.3). (4) The following step is to use a sample of the ground points to create a buffer in which the relative percentage of the classes of vegetation, swimming pools and bare soil are estimated from the

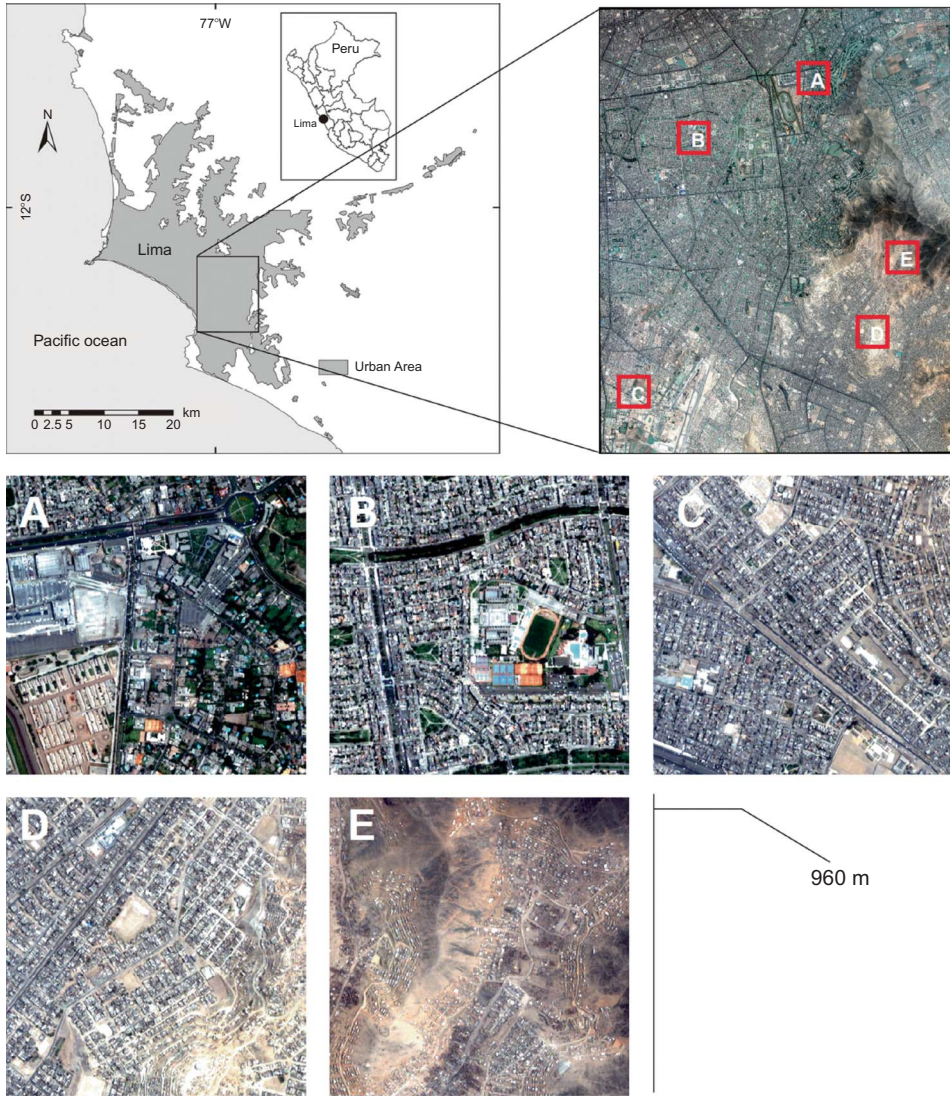


Figure 1. Location of the Lima QuickBird scene featuring some samples of typical urban layouts for socioeconomic classes. All five snapshots have the same relative size ( $960 \times 960$  m).

satellite image (section 3.4). Within this step, the entropy image is used to mask homogeneous, non urban areas, thus refining the selection. (5) The relationship between socioeconomic classes and the satellite observables are then modelled using a neural network (section 3.5). (6) Finally, the trained net is applied to every pixel of the image to generate the socioeconomic classification of the satellite image (section 4).

### 3.1 Data fusion

Several previous tests (not shown) demonstrated the need to improve the spatial resolution of the image to reduce errors in the classification algorithms. This can be

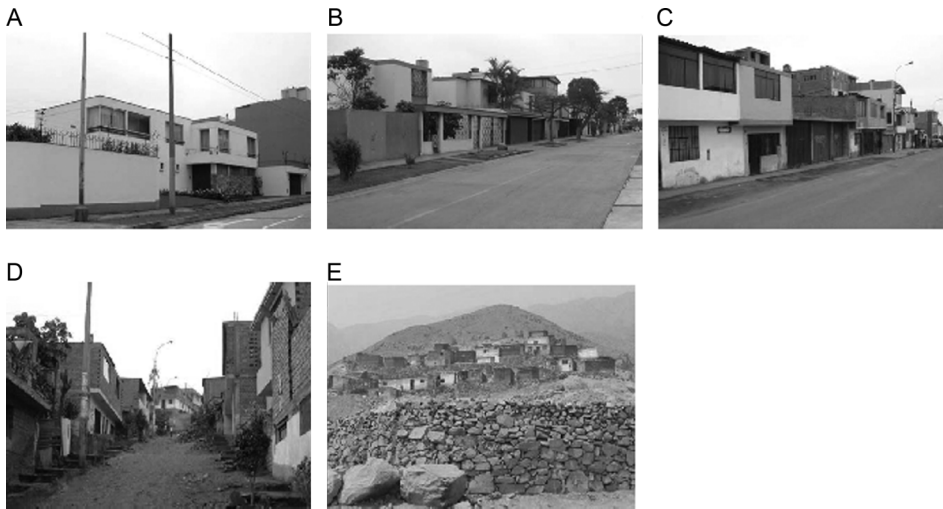


Figure 2. Ground truth of the five major socioeconomic classes used in this study.

achieved using a data fusion procedure. The rationale of fusing multispectral and panchromatic QuickBird imagery is to take advantage of the high spatial resolution of the single panchromatic band and the discrimination capabilities of the multispectral bands, which are of coarser spatial resolution. In other words, the idea is to insert the fine-scale detail provided by the panchromatic band in the multispectral colourful combination, so a new synthetic high-resolution colour image can be generated.

Principal Components Spectral Sharpening (Welch and Ahlers 1987) was used to improve the multispectral image data with the high spatial resolution panchromatic data. This method performs a principal component (PC) transformation of the multispectral data, then replaces the first component, which is the component that has the most variance of image, with the panchromatic image. The panchromatic image is normalized using the histogram of the first PC and conserving the range of this component, aiming to conserve radiometry. Then, the result is resampled to the panchromatic resolution using a cubic convolution algorithm.

While other data fusion methods have been described (Mangolini *et al.* 1995, Wald 1999), the PC technique has the advantage of simplicity and speed, being implemented on many remote sensing packages such as ENVI (ITT Visual Information Solutions, Boulder, CO, USA) or ERDAS Imagine (ERDAS, Inc., Norcross, GA, USA). Examples of PC use are found in El-Askary *et al.* (2005) and in Karathanassi *et al.* (2007), where principal component analysis (PCA) is compared with intensity-hue-saturation (IHS) and Brovey transforms, the Gram-Schmidt fusion method, local mean matching, least square fusion; and discrete wavelet fusion methods including Daubechies, Symlet, Coiflet and biorthogonal spline amongst others. The results in that article for QuickBird imagery showed that PCA had similar performances to local mean matching (LMM), Brovey, Brovey-Colour Normalized (CN), Gram-Schmidt and IHS methods in terms of correlation.

Figure 4 illustrates the visual improvement of the RGB image when the panchromatic data are embedded into the multispectral bands. The results for the PCA fusion are convincing. With the panchromatic image alone (figure 4, left column) it is impossible to distinguish many elements of the image. As an example, it would be hard to

Table 1. Characteristics of social classes in Lima, Peru. Original census data in the city are recorded at household-scale.

Census data	Socioeconomic classes				
	A	B	C	D	E
No. of people per family	3.6	4.1	4.5	4.7	4.6
Family income per month (US\$)	Over 2712	745–2712	325–745	Approx. 239	Approx. 163
Food expenses per month (US\$)	414	84	142	121	117
Transportation expenses per month (US\$)	224	82	51	33	31
No. of bedrooms	3.0	2.7	2.3	2.0	1.7
No. of bathrooms	4.0	2.0	1.2	0.8	0.3
<i>Physical features</i>					
Houses	Large 2-floor houses	Medium size 2-floor houses	Small to medium size 2-floor houses	Small size 1 or 2-floor unfinished houses	Small size 1-floor unfinished houses
Gardens/Swimming pools	Large green areas and large swimming pool	Some green areas and small swimming pool	Not usually green areas or swimming pool	No green areas and no swimming pool	No green areas and no swimming pool
Garage	2 or more cars	1 or 2 cars	Not usual	No	No
Walls	Wall and fences	Wall and fences	No	No	No
Streets	Paved	Paved	Paved – low quality asphalt	Paved – low quality asphalt – or unpaved	Unpaved

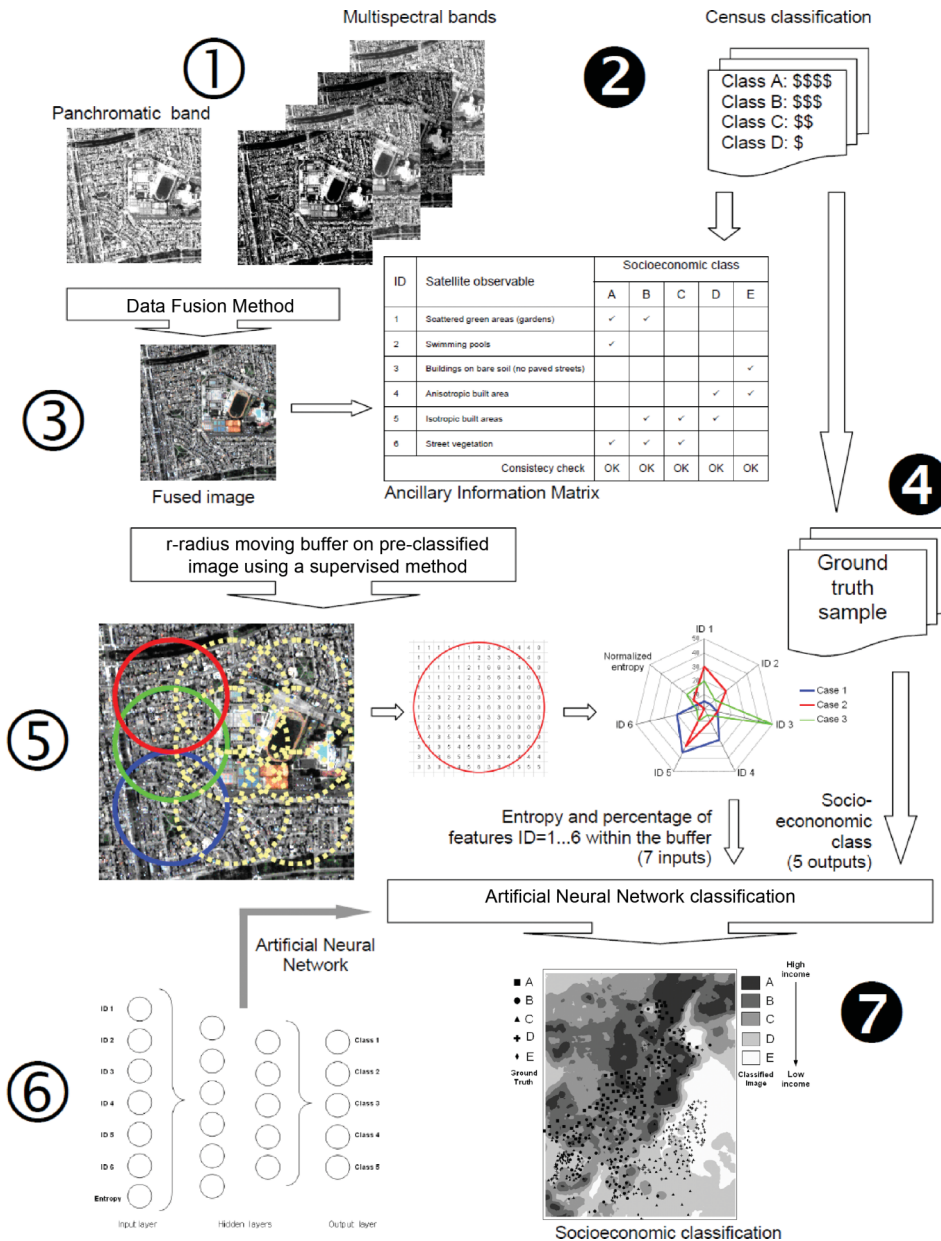


Figure 3. Flow diagram of the methodology proposed in this article.

distinguish swimming pools from other squared elements on the image. Also, lawns can easily be mistaken for bare, flat soil. The multispectral imagery (middle column images) permits us to differentiate such elements thanks to the colour provided by the RGB combination of the bands, but the detail is poor. By contrast, the fused image (figure 4, right column) combines the high-resolution physiographic characteristics of the panchromatic with the radiometric capabilities of the multispectral, producing an improved image that is suitable for classification.

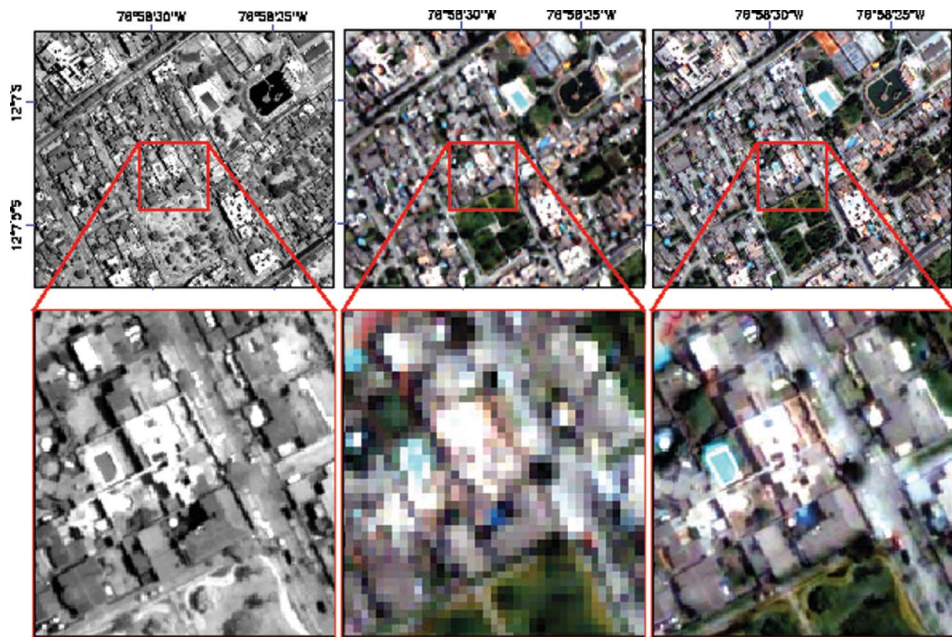


Figure 4. Fused multispectral+panchromatic imagery using the principal component (PC) data-fusion technique. Information from the single, high resolution (0.6 m) panchromatic channel (left) is embedded into the multispectral, lower resolution (2.4 m) red-green-blue (RGB) colour combination (middle) to generate a simulated high resolution (0.6 m) multispectral image (right).

### 3.2 Prior classification

**3.2.1 Classification step.** Most of the techniques relating remote sensing data and socioeconomic information rely on some sort of prior classification of the satellite data. Thus, several techniques have been employed or developed to classify urban images that take into account various class boundaries and within-class variances. They include segmentation algorithms (Taubenbock *et al.* 2006), neural networks (Benediktsson *et al.* 1990, Zhang and Foody 2001, Tapiador and Casanova 2003), non-linear regression (Landis and Koch 1977), support vector machines (Cristianini and Shawe-Taylor 2000), random forests (Breiman 2001), spectral mixture analysis (first described by Adams and Smith 1986, Lu *et al.* 2003) and statistical algorithms such as maximum likelihood (Stefanov *et al.* 2001).

After several tests, the Mahalanobis distance algorithm (described in Richards 1999) was used. This is a supervised technique requiring a few training samples for each class, and a qualitative comparison with other methods concluded that it had a good ability to distinguish classes in the Lima case.

**3.2.2 Satellite observables.** The aim of this classification stage is to transform satellite radiances to satellite observables that could be related with socioeconomic parameters. Those satellite observables include land use categories and spatial structure variables such as isotropy. Knowledge of the local specificities is needed to select those observables. Thus, for example, Lima lies in a very dry environment (less than

2 mm/month of rainfall in August, the rainiest month) so urban vegetation can only be associated with irrigation and thus linked to moderate or high-income areas. Private swimming pools are a luxury that characterizes the upper socioeconomic segment of the population, and slums do not have paved roads. Satellite observables have also to be chosen in a way that they reflect key differences between classes. The matrix relating satellite observables and socioeconomic classes has to pass a consistency check consisting in that the signature of every socioeconomic class has to be different to every other socioeconomic class. The consistency matrix for the Lima case is illustrated in figure 3. The consistency check is required to extrapolate the method presented here to other areas. The procedure is first to choose a sensible set of satellite observables and then fill out the matrix, deciding whether or not the socioeconomic class relates to the satellite observable. If so, then every column has to be compared with each other to confirm that they are all different. If this is not the case, then a different set of observables is needed.

In some cases the observables would differ from the ones used here. Vegetation, however, seems to be an element to look at. Emmanuel (1997) showed the usefulness of satellite-derived vegetation change and demographic trends in cities, also illustrating the usefulness of this element to trace health relationships. Also, Mennis (2006) and Jensen *et al.* (2004) have highlighted vegetation as a relevant element to investigate varied socioeconomic parameters such as population density or home price structure. It has to be noted here that the data fusion procedure was crucial to improve the definition of street vegetation and paved streets.

### 3.3 Entropy calculation

Entropy analysis was used to help the classification algorithm by masking non-built up areas and to calculate the anisotropy of the image. The entropy of ( $S$ ) the image is defined as:

$$S \equiv - \sum_{x \in B((i,j),r)} f(x) \log [f(x)]. \quad (1)$$

where  $f(x)$  is the occurrence (frequency) of the digital level  $x$  in a  $r$ -radius neighbourhood  $B$  centred at coordinates  $(i, j)$ . Therefore, in an urban area entropy is high in inhomogeneous areas and low in homogeneous areas such as soccer fields, bare soils or parks.

The entropy image is built by applying equation (1) in a moving average across the panchromatic image using a 150 m  $r$ -radius. This particular distance is chosen taking into account that the variance in the semivariogram at QuickBird resolution is stable well before 150 m, so the distance represents a large value above which it is extremely unlikely to find large spatial variability. A subsample of the entropy image is depicted in figure 5(b). No quantitative accuracy assessment was conducted on this mask. In terms of qualitative analysis, dark blues to greens represent areas with low entropy, whereas orange, red and white areas are of high entropy. Comparison with the panchromatic image (figure 5(a)) shows that dwelling areas correspond to high entropy areas.

The idea behind using entropy for masking is to help the classification algorithm by removing data that do not introduce useful information into the classification algorithm. That is, entropy is used to differentiate features that are only distinguishable on

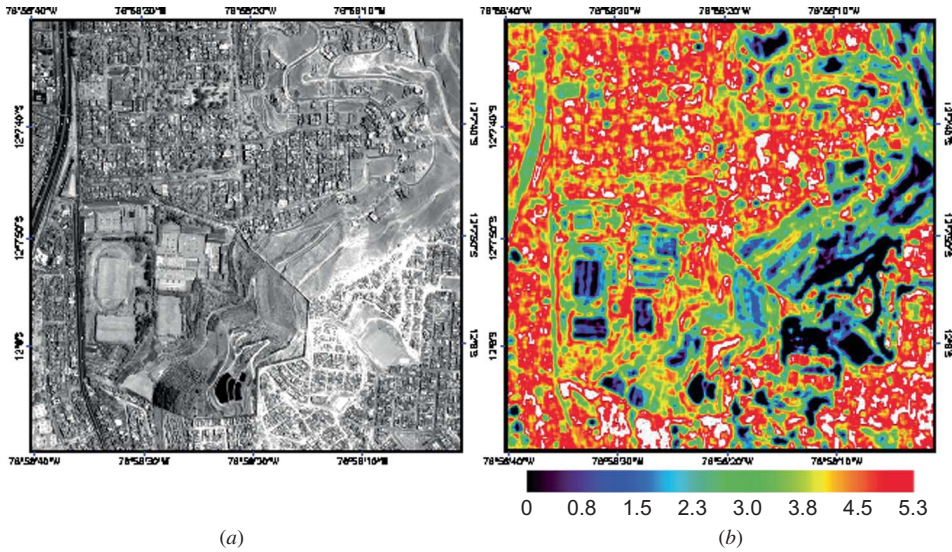


Figure 5. Panchromatic sector of Lima, (a) Peru and (b) its corresponding spatial entropy.

a textural and not on a radiometric basis. As the multispectral image has only four bands, this pre-processing is crucial to avoid contradictory samples. While hyperspectral sensors would allow a best discrimination of urban morphology (Benediktsson *et al.* 2005), the four bands of the QuickBird have a more limited capability of distinguishing the actual fabrics and a coarse-grain approach is needed. The entropy layer allows discrimination between individual trees and gardens associated with high income dwellings and parks or playgrounds using a threshold value of 3.8. The entropy also allows us to filter out motorways near low income dwellings, which may introduce a distorting effect if they are counted as paved surface. The same applies for large official buildings, industries or stores. Several tests showed that this screening of non-housing areas is critical to avoid misclassifications.

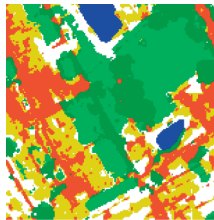
### 3.4 Assignment

The next step was to assign socioeconomic characteristics to the classified image. Given the uncertainties in the ground data collection due to subjective expert appraisal, and the high spatial resolution of the imagery, a naïve pixel-by-pixel approach would not yield the appropriate results, so a strategy has to be devised. Therefore, buffers of 150 m around each ground sample point were defined. This procedure is equivalent to defining a 7-dimensional phase space for each buffer, as the polar diagram (also known as a spiderweb) in figure 6 illustrates for a random case. The spiderweb shows the nature of the heterogeneity within the buffer zone around each target pixel, and represents the link between satellite observables and socioeconomic classes. In practice, this diagram is a large numerical matrix containing the relative proportions of satellite observables and the entropy within a buffer from every pixel in the image. Figure 6 is a graphical representation of the logic behind the buffering procedure. Each socioeconomic class has its own fingerprint in this diagram, but the large number of possible situations and conflicting cases hinder a direct

Fused image (panchromatic+multispectral)



Pre-classified image (Mahalanobis algorithm)



Polar diagram signature

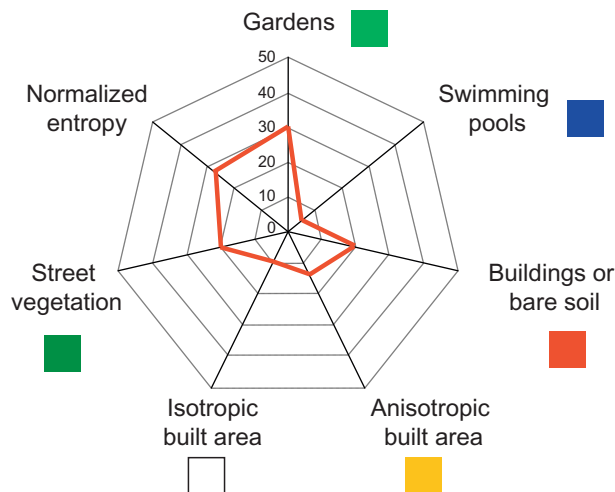


Figure 6. Diagram illustrating a specific pixel-centred buffer and its signature in the polar diagram (step 5 in figure 3). The polar diagram shows the nature of the heterogeneity within the buffer zone around each target pixel.

match between observables and census classes. Therefore, it is necessary to use a robust classification method to resolve mixed cases.

### 3.5 Neural network classifier

The resulting 7-dimensional buffers and the ground data samples were then used as the input/output for a neural network. Thus, the relative percentages of each classification

class were used as the NN input dataset, and the socioeconomic characterizations of that area, as given by the census estimate, were used as the output dataset.

To analyse the performances of the neural net, the dataset was split into training and validation sets. Census class A would be associated with the presence of many green areas and many water bodies (mainly swimming pools in the study area); class B is related to the presence of some green areas and a few water bodies; class C has some green areas, but no water bodies and a limited number of paved roads. Classes D and E correspond to few green areas, no water bodies and more slums than houses; and with few green areas, no water bodies and absence of paved roads, respectively. Nonetheless, this information was not directly used. Rather, the neural network was allowed to freely relate the classification results with the census classes using a training dataset. This allows the NN to find nonlinear relationships between satellite observables and socioeconomic classes.

The neural network used was a simple multilayer perceptron. This particular choice is motivated by the generalization capabilities of this structure and the possibility of calculating the Jacobian of the transformation and thus to perform sensitivity analyses if required. The net consisted of 4 layers, with a 7-6-6-5 arrangement. This structure permits a good generalization capability and the existence of nonlinear relationships between inputs. Training time is below one minute, with an  $R^2$  correlation above 0.80 for the validation data. The trained net was then applied to every pixel of the image to generate the classified image. Given that a buffer has to be generated for each pixel, this step takes about 1 day of computing time in a standard one-processor desktop computer. The NN outputs for the testing dataset were considered as probabilities of an input belonging to a class, so raw output from the NN was truncated to yield actual classes.

## 4. Results and discussion

### 4.1 Lima case study

The results are shown in figure 7, which extends beyond the ground sampling area used in the study to cover the whole QuickBird scene. Figure 7 depicts both the ground-truth data and the classified image. The overall agreement is noticeable given the simple assumptions made (see section 3.2) and the potential problems regarding the influence of shadow, recoding angle, recording date and phenology. This provides empirical evidence about the existence of relationships between socioeconomic characteristics and the urban layout.

A quantitative appraisal of the results is shown in figure 8. Here, the results at 500 m resolution were aggregated, calculating the dominant class for each pixel for both the ground truth validation data and the classified image. The area corresponds with the location boundary of the ground data shown in figure 7. The correlation for those non-masked pixels is high (0.70  $R^2$ ).

Figure 9 shows the histograms of the classes. Within an overall agreement, the method works better in defining the extreme classes (very rich and very poor) rather than the middle classes represented by the C class. Calculations include the producer and user accuracies, the commission and omission errors, the overall accuracy, the kappa quadratic weighting coefficient with error, confidence limits and observed proportion of the maximum possible kappa; and the Spearman's rank coefficient (Spearman 1904). Table 2 shows those statistics. It should be noted that these results have to be taken with caution as such accuracy, commission and omission estimates

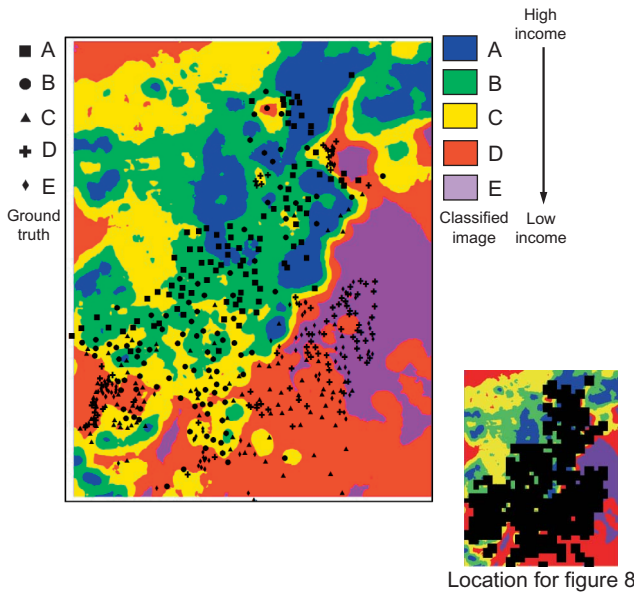


Figure 7. Socioeconomic classification of the multispectral image, with ground-truth data superimposed. The extent of the image corresponds with the whole satellite image (figure 1, top-right), with the area of interest being the sampled area.

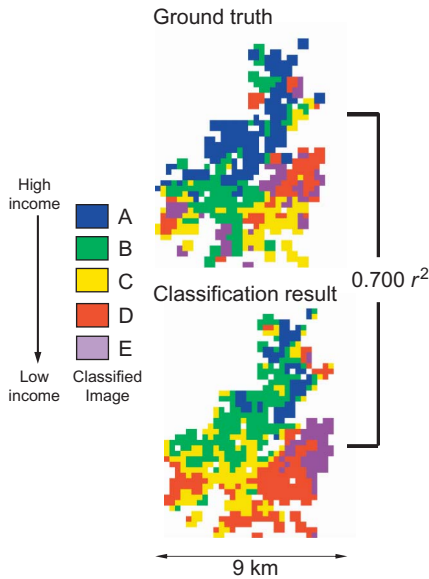


Figure 8. Comparison between the satellite-based socioeconomic classification of figure 5 (bottom) and the ground-truth data (top). The colour scale is the same as in figure 6. Each box represents the predominant class in a 500 m grid.

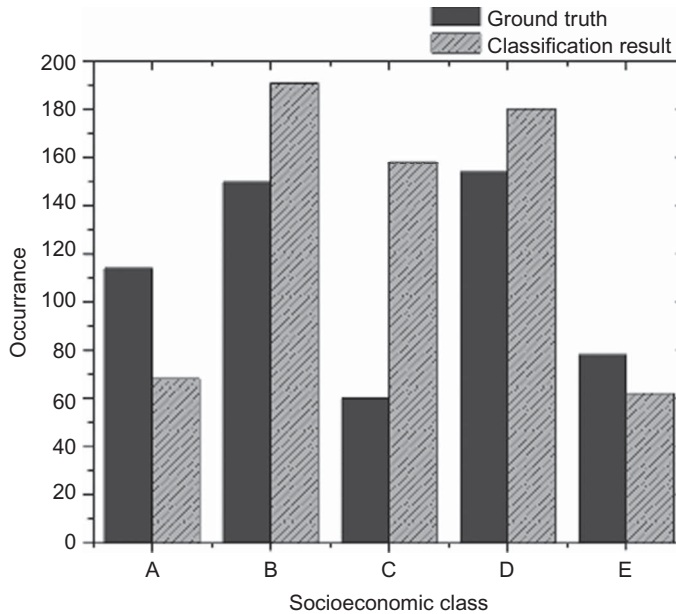


Figure 9. Performances of the described procedure in terms of histogram comparison for each socioeconomic class.

are only suitable for nominal categories (Fleiss 1981). In the case of socioeconomic classes it is meaningful to consider not only the absolute hits, but also the relative concordances. Kappa quadratic weighting accounts for the classification skill of ranks, these being therefore more indicative of the relative merits of the method (Agresti 1996). The comparison yields a 0.70  $R^2$  correlation when compared with the validation data, a moderate value for quantitative data but high for class comparison with Spearman's score and kappa statistic. In terms of rank, the value obtained for Spearman's coefficient (0.67) indicates a strong and positive rank correlation, and the same applies to kappa statistics. In terms of Landis and Koch (1977) scores, the kappa value of  $0.60 \pm 0.03$  (95% confidence limit from 0.54 to 0.66) lies between a moderate (0.41–0.60) and substantial agreement (0.61–0.80).

To summarize the statistical results, they reflect that the method presents a good classification skill, but one that is far from perfect. In fact, it would have been surprising to obtain nearly perfect scores given the small amount of preprocessing required by the method in order to be as general as possible. The features of the empirical data also condition the statistics that could be expected from any classification procedure. First, mixed classes can be found in neighbouring areas. Figure 7 shows that there is little spatial clustering in the ground data to help any classification procedure. Associated with this, another problem is the uncertainties in gathering quality ground data. A third reason is the inherent difficulties in relating satellite information with socioeconomic ground truth. Urban features have proved to be a reasonable proxy for rent but exceptions exist and similar layouts may encompass widely different situations. The method assumes minimum class mobility, but people may have chosen not to move even if they have ascended in the socioeconomic ladder. Also, it is not uncommon to see close rich and poor houses separated by a simple fence. These issues hinder any

Table 2. Omission/commission errors, accuracies and statistics for the classification results.

Census class	Errors of commission	Errors of omission	Producer accuracy	User accuracy
A	90.35	63.33	36.66	9.64
B	65.33	64.86	35.13	34.66
C	81.66	92.02	7.97	18.33
D	54.54	60.67	39.32	45.45
E	70.51	62.90	37.09	29.48
Overall accuracy		0.30		
Observed kappa		0.60 with standard error of 0.03 and 95% confidence limit from 0.54 to 0.66		
Maximum possible kappa given observed marginals		0.782		
Observed proportion of maximum possible		77.26%		
Spearman's rank order correlation		0.67		
$R^2$ correlation		0.70		

high-resolution classification method unless an obvious spatial relationship exists or a raw classification (poor people/rich people) is sought.

#### 4.2 *Applicability to large cities in developing countries*

The methodology is applicable to other areas by either using the satellite observables or by defining a new set of observables and ensuring that the consistency check holds. Unpaved roads in high-entropy urban areas are almost universally linked with deprived dwellings, and poor people can seldom afford a private swimming pool in the backyard. The case of vegetation is more critical as it depends on local climate. In Lima, irrigation is needed, so this element can be used to segment the population into people who live in areas where public services keep public gardens and avenue vegetation alive, and those living in areas where public services are limited. Private gardens in large cities, on the other hand, are more generally related to the middle-upper classes.

As an illustration of the first steps in applying the methodology, figures 10 and 11 depict the corresponding consistency checks for Cairo and Rio de Janeiro. They correspond with an arid and a tropical environment, respectively. QuickBird samples of the five socioeconomic classes are also depicted in the figures. In those two cases, the satellite observables are the same as in the Lima case, which illustrates the applicability of the same rationale to other areas. In the tropical climate of Rio de Janeiro, vegetation is less conspicuously related to social class, which is reflected in the matrix. Another difference appears in the anisotropic built areas. Even so, the consistency check holds, as there are other key elements to differentiate between classes. Applying the method to other areas may require modifying step 4 to account for local specificities. The only requirement is that every socioeconomic class has to have a different signature in term of satellite observables. If this is the case, then it is possible for a classification algorithm to discriminate the classes. Otherwise, the problem has no solution and a different set of observables has to be used.

## Cairo, Egypt

ID	Satellite observable	Socioeconomic class				
		A	B	C	D	E
1	Scattered green areas (gardens)	✓	✓			
2	Swimming pools	✓				
3	Buildings on bare soil (no paved streets)					✓
4	Anisotropic built area				✓	✓
5	Isotropic built areas		✓	✓	✓	
6	Street vegetation	✓	✓	✓		

Class differences	A	B	C	D	E
	A		2,5	1,2,5	1,2,4,5,6
B			1	1,4,6	1,3,4,5,6
C				4,6	3,4,5,6
D					3,5
E					

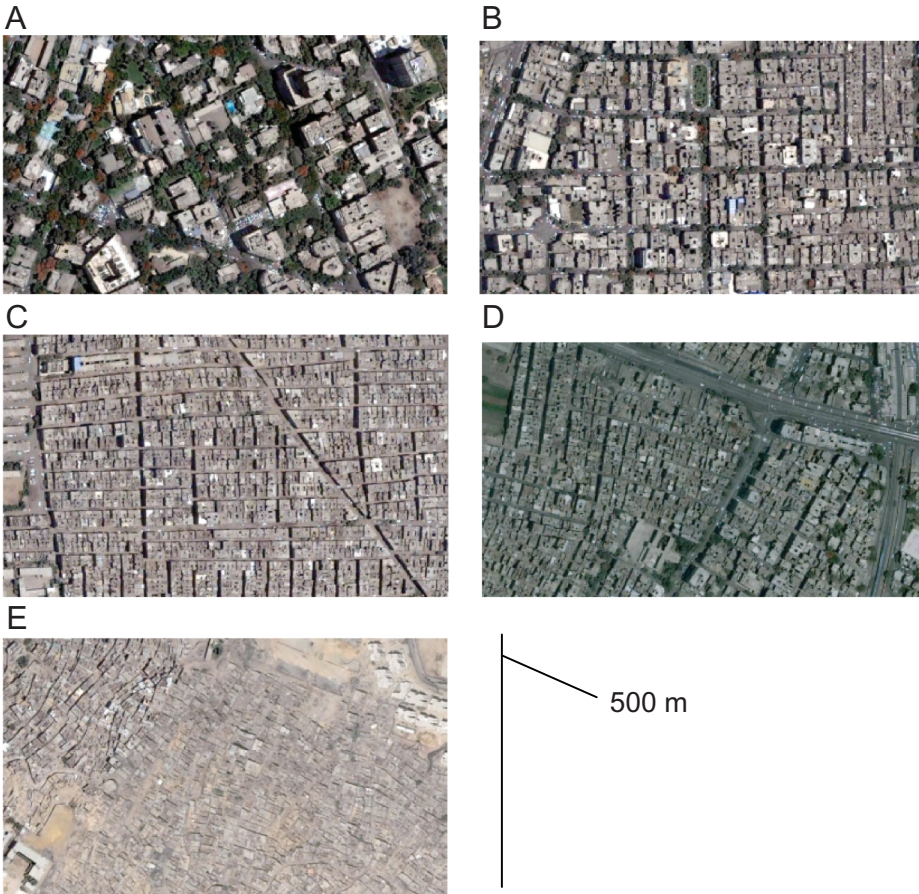


Figure 10. An example of the application of the methodology to the city of Cairo. The satellite observables are the same as in the Lima case. The matrix is consistent as every column has a different signature. The small matrix illustrates the pairwise differences between classes in terms of satellite observables. The images are QuickBird views of the areas corresponding to the five socioeconomic classes.

## Rio de Janeiro, Brazil

ID	Satellite observable	Socioeconomic class				
		A	B	C	D	E
1	Scattered green areas (gardens)	✓	✓			
2	Swimming pools	✓				
3	Buildings on bare soil (no paved streets)					✓
4	Anisotropic built area	✓			✓	✓
5	Isotropic built areas		✓	✓	✓	
6	Street vegetation	✓	✓	✓	✓	✓

Class differences	A	B	C	D	E
	A		2,4,5	1,2,4,5	1,2,5
B			1	1,4	1,3,4,5
C				4	3,4,5
D					3,5
E					

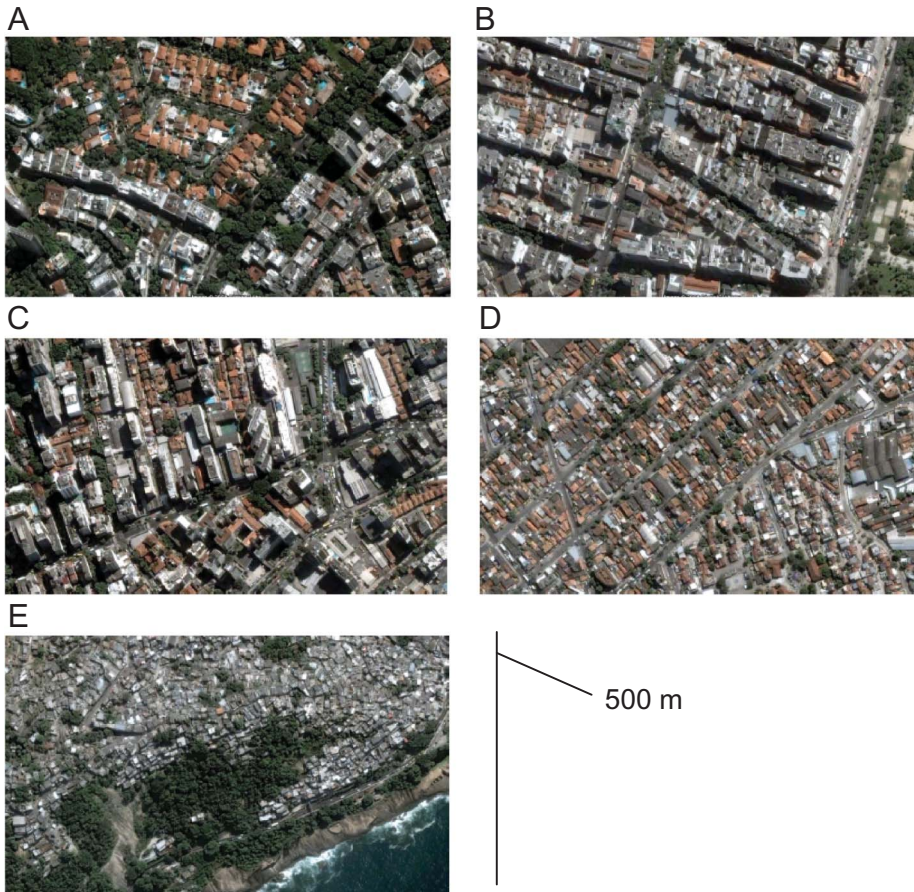


Figure 11. An example of the application of the methodology to the Rio de Janeiro. The satellite observables are the same as in the Lima case. The matrix is consistent as every column has a different signature. The small matrix illustrates the pairwise differences between classes in terms of satellite observables. The images are QuickBird views of the areas corresponding to the five socioeconomic classes.

## 5. Conclusions

Deriving fine-scale social characteristics from satellite imagery is a difficult task. Satellite images are radiometric measurements of the Earth, and the link between those and indicators such as quality of life or income can only be an indirect relationship. Nonetheless, the usefulness of the task has prompted the development of several procedures over recent years.

Here a procedure aiming to derive fine-scale social characteristics from high-resolution QuickBird images has been presented. The procedure can be summarized as a data-fusion merging between panchromatic and multispectral bands aiming to improve the spatial resolution of an automatic land-cover classification of the image, which is then followed by a second supervised classification using a neural network and ground-truth socioeconomic data. While the use of texture measures in urban feature delineation is not new (Carleer and Wolff 2004, Puissant *et al.* 2005), one difference is the use of the entropy to mask out homogeneous areas that would introduce at best contradictory samples into classifying algorithms. The method relies on a further neural network class assignment using ground samples of the desired social classes.

Applications of this method range from a quick preliminary classification of large areas to multitemporal analyses of urban evolution. From a planning perspective, the method can be used to identify deficiencies in municipal services, to monitor social policies and as complementary information to decision-making in urban planning. Nonetheless, deriving socioeconomic information from satellite imagery that might be useful for planning is far from being a fully automated procedure. The results presented here show that a relationship can be found between satellite data and socioeconomic ground information. The distinctive characteristics of the study area should be taken into account when defining the simple parameterization required to link physiographic features with socioeconomic classes. In the Lima case, swimming pools, bare soils and vegetation are three important parameters, which may vary in other megalopolises, especially regarding the role of vegetation.

## Acknowledgments

Francisco Tapiador acknowledges support from projects CGL2010-20787-C02-01 and -02 (Ministerio de Ciencia e Innovación) and PPII10-0162-554 (JCCM).

## References

- ADAMS, J.B. and SMITH, M.O., 1986, Spectral mixture modelling: a new analysis of rock and soil types at the Viking Lander 1 Site. *Journal of Geophysical Research*, **91**, pp. 8098–8112.
- AGRESTI, A., 1996, *An Introduction to Categorical Data Analysis* (New York: Wiley).
- AVELAR, S., ZAH, R. and TAVARES-CORRÊA, C., 2009, Linking socioeconomic classes and land cover data in Lima, Peru: assessment through the application of remote sensing and GIS. *International Journal of Applied Earth Observation and Geoinformation*, **11**, pp. 27–37.
- BENEDIKTSSON, J.A., PALMASON, J.A. and SVEINSSON, J.R., 2005, Classification of hyperspectral data from urban areas based on extended morphological profiles. *IEEE Transactions on Geoscience and Remote Sensing*, **43**, pp. 480–491.
- BENEDIKTSSON, J.A., SWAIN, P.H. and ERSOY, O.K., 1990, Neural network approaches versus statistical methods in classification of multisource remote sensing data. *IEEE Transactions on Geoscience and Remote Sensing*, **28**, pp. 540–552.
- BREIMAN, L., 2001, Random forests. *Machine Learning*, **45**, pp. 5–32.

- BROWN, M.E., 2006, Assessing natural resource management challenges in Senegal using data from participatory rural appraisals and remote sensing. *World Development*, **34**, pp. 751–767.
- CARLEER, A. and WOLFF, E., 2004, Exploitation of very high resolution satellite data for tree species identification. *Photogrammetric Engineering and Remote Sensing*, **70**, pp. 35–140.
- CRISTIANINI, N. and SHAW-TAYLOR, J., 2000, *An Introduction to Support Vector Machines and Other Kernel-based Learning Methods* (Cambridge: Cambridge University Press).
- DOLL, C.N.H., MULLER, J.P. and ELVIDGE, C.D., 2000, Night-time imagery as a tool for global mapping of socioeconomic parameters and greenhouse gas emissions. *AMBIO*, **29**, pp. 157–162.
- EL-ASKARY, H., AGARWAL, A., EL-GHAZAWI, T., KAFATOS, M. and LE-MOIGNE, J., 2005, Enhancing dust storm detection using PCA based data fusion. In *Proceedings of Geoscience and Remote Sensing Symposium*, 25–29 July 2005, Seoul, South Korea, vol. 2, pp. 1424–1427.
- EMMANUEL, R., 1997, Urban vegetational change as an indicator of demographic trends in cities: the case of Detroit. *Environment and Planning B*, **24**, pp. 415–426.
- FAUVEL, M., CHANUSSOT, J. and BENEDIKTSSON, J.A., 2006, Decision fusion for the classification of urban remote sensing images. *IEEE Transactions on Geoscience and Remote Sensing*, **44**, pp. 2828–2838.
- FLEISS, J.L., 1981, *Statistical Methods for Rates and Proportions*, 2nd edn (New York: John Wiley).
- FOODY, G.M., 2002, Status of land cover classification accuracy assessment. *Remote Sensing of Environment*, **80**, pp. 185–201.
- FOX, J., RINDFUSS, R.R., WALSH, S.J. and MISHRA, V. (Eds.), 2003, *People and the environment: approaches for linking household and community surveys to remote sensing and GIS* (Norwell, MA: Kluwer Academic).
- HENDERSON, F.M. and XIA, Z.G., 1997, SAR applications in human settlement detection, population estimation and urban land use pattern analysis: a status report. *IEEE Transactions on Geoscience and Remote Sensing*, **35**, pp. 79–85.
- HEROLD, M., HEMPHILL, J. and CLARKE, K.C., 2007, Remote sensing and urban growth theory. In *Urban Remote Sensing*, Q. Wang and D.A. Quattrochi (Eds.) (Boca Raton, FL: CRC Press).
- HUANG, C., DAVIS, L.S. and TOWNSHEND, J.R.G., 2002, An assessment of support vector machines for land cover classification. *International Journal of Remote Sensing*, **23**, pp. 725–749.
- JENSEN, J.R. and COWEN, D.C., 1999, Remote sensing of urban/suburban infrastructure and socio-economic attributes. *Photogrammetric Engineering and Remote Sensing*, **65**, pp. 611–622.
- JENSEN, R., GATRELL, J., BOULTON, J. and HARPER, B., 2004, Using remote sensing and geographic information systems to study urban quality of life and urban forest amenities. *Ecology and Society*, **9**, p. 5.
- KARATHANASSI, V., KOLOKOUSIS, P. and IOANNIDOU, S., 2007, A comparison study on fusion methods using evaluation indicators. *International Journal of Remote Sensing*, **28**, pp. 2309–2341.
- LANDIS, J.R. and KOCH, G.G., 1977, The measurement of observer agreement for categorical data. *Biometrics*, **33**, pp. 159–174.
- LI, G. and WENG, Q., 2007, Measuring the quality of life in city of Indianapolis by integration of remote sensing and census data. *International Journal of Remote Sensing*, **28**, pp. 249–267.
- LO, C.P., 2002, Urban indicators of China from radiance-calibrated digital DMSP-OLS nighttime images. *Annals of the Association of American Geographers*, **92**, pp. 225–240.

- LO, C.P. and FABER, B.J., 1997, Integration of Landsat Thematic Mapper and census data for quality of life assessment. *Remote Sensing of Environment*, **62**, pp. 143–157.
- LU, D., MORAN, E. and BATISTELLA, M., 2003, Linear mixture model applied to Amazonian vegetation classification. *Remote Sensing of Environment*, **87**, pp. 456–469.
- MANGOLINI, M., RANCHING, T. and WALD, L., 1995, Evaluation de la qualité des images multispectrales à haute résolution spatiale dérivées de SPOT [Quality evaluation of SPOT multispectral imagery at high spatial resolution]. *Bulletin Société Française de Photogrammétrie et Télédétection*, **137**, pp. 24–29 [in French].
- MARTINUZZI, S., GOULD, W.A. and GONZALEZ, O.M.R., 2007, Land development, land use, and urban sprawl in Puerto Rico integrating remote sensing and population census data. *Landscape and Urban Planning*, **79**, pp. 288–297.
- MENNIS, J., 2006, Socioeconomic-vegetation relationships in urban, residential land: the case of Denver, Colorado. *Photogrammetric Engineering and Remote Sensing*, **72**, pp. 911–921.
- MESEV, V., 2003, *Remotely Sensed Cities* (London: Taylor & Francis).
- POZZI, F. and SMALL, C., 2005, Analysis of urban land cover and population density in the United States. *Photogrammetric Engineering and Remote Sensing*, **71**, pp. 719–726.
- PUISSANT, A., HIRSCH, J. and WEBER, C., 2005, The utility of texture analysis to improve per-pixel classification for high to very high spatial resolution imagery. *International Journal of Remote Sensing*, **26**, pp. 733–745.
- RICHARDS, J.A., 1999, *Remote Sensing Digital Image Analysis* (Berlin: Springer-Verlag).
- SETO, K.S. and KAUFMANN, R.K., 2003, Modeling the drivers of urban land use change in the Pearl River Delta, China: integrating remote sensing with socioeconomic data. *Land Economics*, **79**, pp. 106–121, doi: 10.2307/3147108.
- SPEARMAN, C., 1904, The proof and measurement of association between two things. *American Journal of Psychology*, **15**, pp. 72–101.
- STEFANOV, W.L., RAMSEY, M.S. and CHRISTENSEN, P.R., 2001, Monitoring urban land cover changes: an expert system approach to land cover classification of semiarid to arid urban centers. *Remote Sensing of Environment*, **77**, pp. 173–185.
- TAPIADOR, F.J. and CASANOVA, J.L., 2003, Land-use mapping methodology using remote sensing for the regional planning directives in Segovia, Spain. *Landscape and Urban Planning*, **62**, pp. 103–115.
- TAUBENBOCK, H., ESCH, T. and ROTH, A., 2006, An urban classification approach on an object-oriented analysis of high resolution satellite imagery for a spatial structuring within urban areas. In *Workshop on SIG Urban Remote Sensing*, 2–3 March 2006, Humboldt-University, Berlin, Germany.
- WALD, L., 1999, Some terms of reference in data fusion. *IEEE Transactions on Geoscience and Remote Sensing*, **37**, pp. 1190–1193.
- WANG, Q. and QUATTROCHI, D.A., 2007, *Urban Remote Sensing* (Boca Raton, FL: CRC Press).
- WEBER, C., 2003, Interaction model application for urban planning. *Landscape and Urban Planning*, **63**, pp. 49–60.
- WELCH, R. and AHLERS, W., 1987, Merging multiresolution SPOT HRV and Landsat TM data. *Photogrammetric Engineering and Remote Sensing*, **53**, pp. 301–303.
- WU, C.S., 2004, Normalized spectral mixture analysis for monitoring urban composition using ETM plus imagery. *Remote Sensing of Environment*, **93**, pp. 480–492.
- ZHANG, G. and FOODY, G.M., 2001, Fully-fuzzy supervised classification of sub-urban land cover from remotely sensed imagery: statistical and artificial neural network approaches. *International Journal of Remote Sensing*, **22**, pp. 615–628.